Lipid-Protein Interactions Alter Line Tensions and Domain Size Distributions in Lung Surfactant Monolayers

Prajnaparamita Dhar,[†*] Elizabeth Eck,[‡] Jacob N. Israelachvili,[‡] Dong Woog Lee,[‡] Younjin Min,[§] Arun Ramachandran,[¶] Alan J. Waring,[‖] and Joseph A. Zasadzinski[**]

[†]Department of Chemical Engineering, University of Kansas, Lawrence, Kansas; [‡]Department of Chemical Engineering, University of California, Santa Barbara, California; [§]Department of Chemical Engineering, Massachusetts Institute of Technology, Cambridge, Massachusetts; [¶]Department of Chemical Engineering and Applied Chemistry, University of Toronto, Toronto, Ontario, Canada; [‖]Departments of Medicine and Pediatrics, UCLA School of Medicine, Los Angeles, California; and **Chemical Engineering and Materials Science, University of Minnesota, Minneapolis, Minnesota

ABSTRACT The size distribution of domains in phase-separated lung surfactant monolayers influences monolayer viscoelasticity and compressibility which, in turn, influence monolayer collapse and set the compression at which the minimum surface tension is reached. The surfactant-specific protein SP-B decreases the mean domain size and polydispersity as shown by fluorescence microscopy. From the images, the line tension and dipole density difference are determined by comparing the measured size distributions with a theory derived by minimizing the free energy associated with the domain energy and mixing entropy. We find that SP-B increases the line tension, dipole density difference, and the compressibility modulus at surface pressures up to the squeeze-out pressure. The increase in line tension due to SP-B indicates the protein avoids domain boundaries due to its solubility in the more fluid regions of the film.

INTRODUCTION

A complex mixture of lipids and proteins, collectively called lung surfactant (1–3), lines the alveoli of mammalian lungs. Synthesized, secreted, and regenerated by type II alveolar epithelial cells, lung surfactants regulate the interfacial tension in the lung air-liquid interfaces, minimizing the work of breathing and ensuring uniform lung inflation (3,4). During expiration, the surfactant film attains near-zero surface tension, which promotes uniform and low energy reinflation during inspiration, while preventing atelectasis, the collapse of the alveoli (3,4). An absence or deficiency of lung surfactant due to immaturity in premature infants leads to neonatal respiratory distress syndrome (3), which is treated by administering animal-derived replacement lung surfactants (4). Acute respiratory distress syndrome, which afflicts 150,000 adults annually in the US, is also linked to surfactant dysfunction (5,6), although the coupling between surfactant dysfunction and the underlying disease is poorly understood. This is due to a lack of understanding of the roles individual lipids and proteins play in creating the monolayer properties necessary to achieve low surface tensions in a biochemically and biophysically challenging alveolar environment (5,6).

Native surfactant contains 90% lipid and 10% (by weight) of four lung surfactant-specific proteins: SP-A, -B, -C, and –D (4,7). SP-B and SP-C are short hydrophobic polypeptides that are essential for normal respiration (4). SP-B deficiency causes lethal respiratory distress at birth in humans and in SP-B knock-out mice (8,9). Although SP-C gene deletion does not have dire consequences at birth, it does lead to pneumonitis in knock-out mice after birth (10,11). SP-A and SP-D are hydrophilic glycoproteins important for host defense, but are removed from clinical surfactants without loss of surface activity (12,13).

Literature reports on the lipid fraction and even the lipid species in lung surfactants are varied, so there is no consensus lung-surfactant composition; as a result, the composition of clinical replacement surfactants also varies (4,7). Disaturated dipalmitoylphosphatidylcholine (DPPC) makes up the dominant fraction of lung surfactant, but ranges from 30% to 80% in literature reports. The remaining lipids include unsaturated phosphatidylcholines (PC, 25–35%), anionic phospholipids such as phosphatidylglycerol (PG), and minor fractions of phosphatidylethanolamine, sphingomyelin (4), and cholesterol. Fatty acids such as palmitic acid are added to Survanta (Abbott Laboratories, North Chicago, IL), although there is little free fatty acid in native surfactant (4,7). Even with this lipid variability, clinical surfactants have similar efficacy for neonatal respiratory distress syndrome treatment but all have been disappointing in treating acute respiratory distress syndrome (5,6).

Proper lung function requires that lung surfactants form low surface tension monolayers on compression (exhalation) but respread and/or adsorb from the subphase quickly during expansion (inspiration). However, no individual lipid or protein monolayer exhibits both these properties. While a solvent-spread DPPC monolayer lowers the surface tension to near zero when fully compressed (14), it fails to adsorb from solution or respread at the necessary rate when the film is expanded. Unsaturated and anionic lipids,

Submitted August 31, 2011, and accepted for publication November 7, 2011.

*Correspondence: prajnadhar@ku.edu

Editor: Ka Yee Lee.

0006-3495/12/01/0056/10 $2.00

doi: 10.1016/j.bpj.2011.11.4007

which fluidize the monolayer, as well as the amphiphilic proteins SP-B and SP-C, work together to promote adsorption and spreading (4). However, unsaturated lipid monolayers cannot achieve the low surface tensions necessary for lung function. In mixtures, the unsaturated lipids and proteins are usually localized in a fluid, liquid-expanded (L_E) phase, interspersed with more rigid, liquid crystalline (L_C) domains in which the saturated lipids reside (14–22). The fluid phase lipids and proteins are believed to be squeezed-out of the monolayer on compression, but they remain attached to (14,17,19–24), or in the vicinity of, the interface in a surface-associated reservoir (25) where they can readsorb during inhalation (21,22). In vivo, electron microscopy of the alveoli (26) and atomic force microscopy of in vitro films (17,19–22,27) show discontinuous multilayer patches along with monolayer films.

Hence, how the monolayer distributes into domains of different fluidity and composition (28–31) has a significant impact on squeeze-out (14–16,24,32–37). Recent work has also shown that the domain morphology and line tension between domains can determine the interfacial viscoelasticity (38–41) (which controls spreading and the rate of collapse) and adsorption from solution or reincorporation of material into the monolayer after collapse (21,22,24,27,36,37,41). The lateral organization of lipid domains strongly couples to membrane properties, such as membrane curvature, that affect membrane stability (32) and the ability of a monolayer film to resist collapse at low surface tensions.

However, there is little quantitative information on the parameters that determine domain size distributions (28,31,42), especially in complex lipid/protein monolayers (30). We have recently shown that two parameters, the dipole density difference, Δm, and the line tension, λ, between the domains and the continuous matrix, uniquely determine a model of the domain size distribution (30). This model (30) is used here to fit the domain size distributions in a clinical lung surfactant film (Survanta), with and without surfactant protein SP-B. From the model, we extracted the dipole density difference and the line tension; to our knowledge, this is the first time that the line tension and the dipole density difference have been measured for a lung surfactant. SP-B increases the line tension and dipole density difference in the monolayer, causing the domain size distribution to become smaller and less polydisperse. This correlates with an increased monolayer compressibility at low surface pressures before squeeze-out, which reduces the compression needed to reach low surface tensions (15,16). The effects of SP-B on the line tension and dipole density difference decrease with increasing surface pressure, consistent with SP-B being gradually removed from the monolayer, or undergoing significant changes in conformation or orientation with increasing surface pressure. This correlates with SP-B's role in facilitating the exchange of the unsaturated lipids with the monolayer-associated reservoir (21,26) during squeeze-out.

Increasing the SP-B concentration increases the line tension; the two-dimensional analog of the Gibbs Adsorption Isotherm (see the Supporting Material for derivation) suggests that SP-B prefers the more fluid regions of the film and is repelled from the domain line boundary and the ordered phase (15–17,19,27,44–47). SP-B cannot pack into the semicrystalline domains and partitions into the fluid phase, just as the fluorescent dye used to generate contrast. Furthermore, an increase in the dipole density difference provides further evidence that SP-B interacts with the anionic PG, which is located in the fluid phase (27). Our results provide a quantitative description of the influence of lipid-protein interactions on the line tension and dipole density difference between domains, how these parameters influence the lateral organization of lipids, and how this influences the properties essential to the normal functions of lung surfactant (15,16).

THEORY

Domain size distributions and monolayer properties

Differences in lipid headgroups, chain length, tilt, or local order at phase boundaries lead to a line tension, λ. Differences in packing or composition between the domains and the continuous phase result in a difference in the average dipole density, Δm, which leads to an electrostatic repulsion within and between domains (30). The energy per molecule, E/N, in an isolated circular domain of radius R ($N = \pi R^2/a_o$, a_o is the average area per molecule) is set by a balance of these opposing forces (28):

$$\frac{E}{N} = \frac{2a_o}{R}\left[\lambda - \frac{(\Delta m)^2}{4\pi\varepsilon\varepsilon_o}\ln\left(\frac{4R}{e^2\delta}\right)\right] = 2a_o\rho\left[\lambda + \frac{(\Delta m)^2}{4\pi\varepsilon\varepsilon_o}\ln\left(\frac{\rho e^2\delta}{4}\right)\right], \quad (1)$$

where $\rho = 1/R$ is the curvature, $\varepsilon \sim 40$ is the dielectric constant for interfacial water, $\varepsilon_o = 8.854 \times 10^{-12}$ C^2/J·m, and $\delta \sim 0.5$ nm is a cut-off distance between the dipolar charges (dipole length) and $e = 2.714$ (28). To compare to the derivations by McConnell (28) or Heinrich et al. (48), $(\Delta m)^2/4\pi\varepsilon\varepsilon_o \equiv (4\mu)^2$. The minimum energy radius, R_o, for an isolated domain is

$$R_o = \frac{1}{\rho_o} = \left(\frac{e^3\,\delta}{4}\right)\exp\left[\frac{[4\pi\varepsilon\varepsilon_o\lambda]}{(\Delta m)^2}\right]. \quad (2)$$

However, in a typical monolayer, domain sizes remain polydisperse for hours (49), suggesting that the entropy of mixing creates a size distribution, similar to distribution of micelles and spontaneous vesicles (50,51). The size

distribution is determined by equating the chemical potential of a lipid molecule in a domain of M molecules, corresponding to R_o ($M = \pi R_o^2/a_o$), with that of a molecule in a domain of N molecules of radius R ($N = \pi R^2/a_o$),

$$\mu_N^0 + \frac{k_B T}{N}\ln\frac{X_N}{N} = \mu_M^0 + \frac{k_B T}{M}\ln\frac{X_M}{M}, \tag{3}$$

where μ_N^0, X_N and μ_M^0, X_M are the standard state chemical potentials and mole fractions of molecules in domains of size N and M, respectively; k_B is the Boltzmann constant (1.38×10^{-23} J·K^{-1}) and T is the temperature (K). This ideal entropy of mixing assumes no interactions between domains, which is true if the domains are sufficiently dilute. Equation 3 can be rearranged as

$$C_N = \left[C_M \exp\left(\frac{M(\mu_M^0 - \mu_N^0)}{k_B T}\right)\right]^{N/M}. \tag{4}$$

The values $C_N = X_N/N$ and $C_M = X_M/M$ are the number fractions of domains with N (radius R) or M (radius R_o) molecules, respectively. We set the standard state chemical potential to the energy of an isolated domain of N or M molecules, and use Eq. 1 to determine $(\mu_M^0 - \mu_N^0)$:

$$C_N = \left[C_M \exp\left[-\left(\frac{(\Delta m)^2 R_o}{4\varepsilon\varepsilon_o k_B T}\right)\left(1 + \frac{R_o}{R}\left(\ln\frac{R_o}{R} - 1\right)\right)\right]\right]^{R^2/R_o^2}. \tag{5}$$

However, in Eq. 5, $C_N \to 1$ as $R \to 0$, due to an overestimate of the entropy relative to the energy. A better approximation that decreases monotonically as $R \to 0$ is possible by expanding Eq. 1 in a Taylor series at $\sim\rho_o = 1/R_o$,

$$\begin{aligned}(\mu_N^0 - \mu_M^0) &= \frac{E}{N} - \frac{E}{M} = \left.\frac{\partial(E/N)}{\partial\rho}\right|_{\rho=\rho_o} \\ &(\rho - \rho_o) + \left.\frac{\partial^2(E/N)}{\partial\rho^2}\right|_{\rho=\rho_o}\frac{(\rho - \rho_o)^2}{2} + \ldots,\end{aligned} \tag{6}$$

where, at $\rho_o = 1/R_o$, the first derivative of the energy is zero. To quadratic order, the chemical potential difference is

$$\begin{aligned}(\mu_N^0 - \mu_M^0) &= \frac{a_o\rho_o(\Delta m)^2}{4\pi\varepsilon\varepsilon_o}(\rho - \rho_o)^2 \\ &= \frac{a_o(\Delta m)^2}{4\pi\varepsilon\varepsilon_o R_o}\left(\frac{1}{R} - \frac{1}{R_o}\right)^2.\end{aligned} \tag{7}$$

As shown in Fig. 1, using the Taylor series expansion to quadratic term is an excellent approximation to the full energy difference around R_o. The energy difference obtained either by using the expression for energy in Eq. 1, or the Taylor series expansion, leads to comparable values around $R = R_0$. Substituting Eq. 7 in Eq. 4:

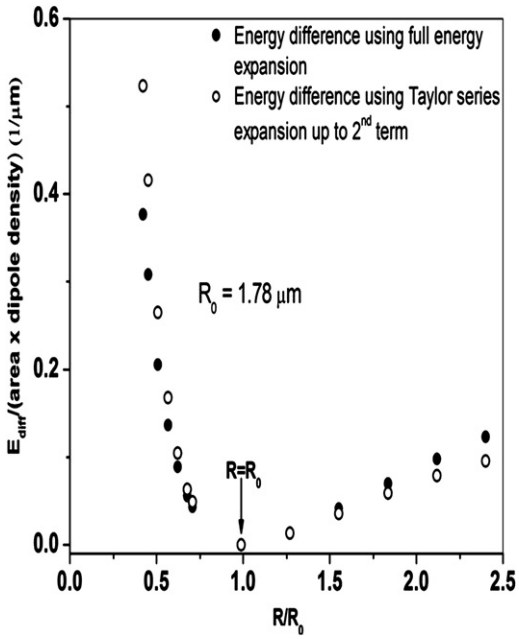

FIGURE 1 Comparison of the full energy difference versus quadratic Taylor series expansion as a function of domain radius, R, for R_o = 1.78 μm. The Taylor series approximation is good from ~R_o/3 to 2.5R_o, the range of the domain sizes typically seen in images such as in Figs. 3 and 4.

$$\begin{aligned}C_N &= \left[C_M \exp\left[-\left(\frac{(\Delta m)^2(\rho/\rho_o - 1)^2}{4\varepsilon\varepsilon_o\rho_o k_B T}\right)\right]\right]^{\rho_0^2/\rho^2} \\ &= \left[C_M \exp\left[-\left(\frac{(\Delta m)^2 R_o(R_o/R - 1)^2}{4\varepsilon\varepsilon_o k_B T}\right)\right]\right]^{R^2/R_o^2}.\end{aligned} \tag{8}$$

Equation 8, which decreases monotonically as $R \to 0$, is used to fit the domain size distribution using C_M, $(\Delta m)^2 R_o/4\varepsilon\varepsilon_o k_B T$, and R_o, as the three independent fitting parameters, from which λ and Δm can be derived (see Eq. 2). Equation 8 was also recently used to model the domain size distribution in myelin membranes (30).

Compressibility modulus and monolayer transitions

The ability of a material to store mechanical (strain) energy when stressed is defined by its bulk (three-dimensional) modulus. By analogy, the two-dimensional isothermal bulk modulus, β, for monolayers is defined as

$$\beta = -A\left(\frac{\partial\Pi}{\partial A}\right)_T = A\left(\frac{\partial\gamma}{\partial A}\right)_T = \frac{1}{\kappa}. \tag{9}$$

The inverse of β is the isothermal compressibility, κ. Because β and κ are second-order derivatives of the free

energy, G, ($\gamma = (\partial G/\partial A)_T$, $\beta = (\partial^2 G/\partial A^2)_T$), a discontinuous change at which $\beta \rightarrow 0$ or $k \rightarrow \infty$ is the signature of a first-order phase transition. Experimentally, phase transitions appear as a dip in the β versus A profile rather than a sharp discontinuity.

MATERIALS AND METHODS

Survanta, an organic extract from minced bovine lungs used to treat neonatal respiratory distress syndrome (Abbott Laboratories, Columbus, OH) (7), was donated by the Santa Barbara Cottage Hospital (Santa Barbara, CA). The lipids and proteins were extracted from the Survanta aqueous suspension with 2:1 chloroform/methanol, followed by washing with normal saline. The chloroform phase containing the surfactant lipids and proteins was concentrated by flash evaporation and the hydrophobic surfactant proteins were separated from the surfactant lipids by Sephadex LH-20 column chromatography (52). The protein fractions were applied to a normal phase liquid chromatography column packed with Silica Octyl (C8) (J.T. Baker, Phillipsburg, NJ) and the SP-B and SP-C were separated by isocratic elution using a solvent system of 7:1:0.4 (v/v) MeOH:$CHCL_3$:H_2O with 0.1% trifluoroacetic acid as an ion pairing agent (53). The molecular mass of the individual protein fractions were confirmed by SDS gel electrophoresis, and matrix-assisted laser-desorption/ionization time-of-flight mass spectrometry (22).

The extracted Survanta lipids were mixed in HPLC grade chloroform with 1 wt % Texas-Red 1,2-dihexadecanoyl-*sn*-glycero-3-phosphoethanolamine, triethylammonium salt (DHPE; Invitrogen, Carlsbad, CA). To add SP-B, the lipids were mixed with 5 wt % of an organic solution of SP-B in 4:1 chloroform: methanol labeled with 1 wt % Texas-Red DHPE. The organic mixtures were dried under nitrogen flow and any remaining solvent was removed by placing in house vacuum overnight. The dried lipid or lipid-protein mixtures were rehydrated to 2 mg/mL in a standard saline buffer (150 mM NaCl, 2 mM $CaCl_2$ 0.2 mM $NaHCO_3$, pH 7.0) by heating overnight at 55°C with continuous gentle agitation. Samples were stored at 5°C.

Surface pressure-area isotherms were recorded at 25°C using a Teflon trough (Nima, Coventry, England) with custom-designed stainless steel ribbons which reduce film leakage at high surface pressures. The surface pressure was recorded with a Wilhelmy plate balance. The open area of the trough used was 125 cm^2 and each complete compression/expansion cycle took ~8 min (0.42 cm^2/s). A total of 800 μg of the different surfactant mixtures was added dropwise into 150 mL of saline buffer in the trough and allowed to equilibrate for 20 min before starting the compression/expansion cycle. Because most of the surfactant is in the bulk subphase, film formation at the interface occurs primarily via adsorption of the surfactant mixture from the subphase. The compressibility modulus was calculated from the isotherm data by calculating the slope (s) using the difference formula

$$S = \frac{1}{2}\left(\frac{(y_{i+1} - y_i)}{(x_{i+1} - x_i)} + \frac{(y_i - y_{i-1})}{(x_i - x_{i-1})}\right), \qquad (10)$$

where x_i and y_i are the values of fractional trough area and surface pressure, respectively, at any point. The numerical derivatives of the surface pressure versus fractional trough area curve were evaluated using the Differentiate tool and smoothed with a Fourier filter using Origin 8.1 (OriginLab, Northampton, MA).

For fluorescence imaging, the Langmuir trough was mounted on an Optiphot optical microscope (Nikon, Melville, NY) with a custom-designed stage equipped with long-working-distance objectives designed for fluorescent light. A dichroic mirror/barrier filter assembly directed the excitation light onto the monolayer films at a normal angle of incidence and filtered the emitted light. The images were detected by a silicon-intensified charge-coupled device camera. Videos of the monolayer film were recorded during the compression-expansion cycle directly onto the computer using Pinnacle Studio video capture software (Pinnacle, Avid, Mountain View, CA). The continuous, fluid lipid phase appears bright while the better-ordered domains exclude the dye molecules and appear dark (28,46).

The domain sizes and distributions were analyzed using the software ImageJ (National Institutes of Health, Bethesda, MD) and plotted as normalized histograms before fitting to Eq. 8 using Origin 8.1 (OriginLab). To increase the quality of the statistics, two neighboring frames were analyzed at each surface pressure. The number of bins was set equal to $n^{1/2}$, in which n is the number of domains counted in the image. The width of the bins was set by dividing the maximum domain size by $n^{1/2}$; the minimum resolved domain radius was 0.5 μm, which was set by the resolution of the optical microscope. The vertical axis of all histograms is represented as relative frequency (i.e., fraction of the total domains that lie within a particular bin size) such that the total area of the histogram is 1, making the histogram a probability distribution. The distribution was fit to Eq. 8 with C_M, $(\Delta m)^2 R_o/4\varepsilon\varepsilon_o k_B T$, and R_o as adjustable parameters, using the Nonlinear Curve Fit feature of Origin 8.1 (OriginLab). We were limited to surface pressures below 40 mN/m because the L_C domains were >50% of the film at higher surface pressures and the contrast between L_C and L_E phases was difficult to visualize (21).

RESULTS

Isotherms

Fig. 2 *a* shows typical quasistatic compression-expansion cyclic isotherms for 800 μg of Survanta (*open squares*), extracted Survanta lipids (*solid squares*), or Survanta lipids plus 5 wt % SP-B (*stars*). The Survanta isotherm displayed a plateau at Π ~ 40–45 mN/m, which is associated with the squeeze-out of unsaturated lipids and the formation of a surfactant reservoir (26) of multilayer films attached to the monolayer (17,20–23,27). The surface pressure reached a maximum pressure Π ~ 67 mN/m (which was maintained during further compression of the film) at a trough area of $A = 0.45$ (45%) of the original expanded area. On expansion, the surface pressure dropped rapidly to 10 mN/m, showing the hysteresis common to most lung surfactants (21,46). The Survanta lipids had a similar isotherm, except that the plateau at Π ~ 40–45 mN/m disappeared. The maximum surface pressure remained at 67 mN/m, but was not reached until the trough was compressed to 0.38 (38%) of the original area. Adding 5 wt % SP-B to the Survanta lipids made small changes in the isotherm; the maximum collapse pressure remained at Π ~ 67 mN/m on compression at an area intermediate between the Survanta lipids and Survanta.

Compressibility modulus

Fig. 2 *b* shows the compressibility modulus, β, versus fractional trough area curves. The compressibility modulus of the Survanta lipids is roughly constant at β ~ 50 mN/m until it peaks at β ~ 210 mN/m, which is associated with monolayer collapse (*solid arrows*). Survanta films showed a broad peak up to β ~ 140 mN/m followed by a sharp dip to β ~ 30 mN/m that corresponds to the characteristic squeeze-out plateau in the isotherm. The collapse peak was similar to that of the Survanta lipids, although the

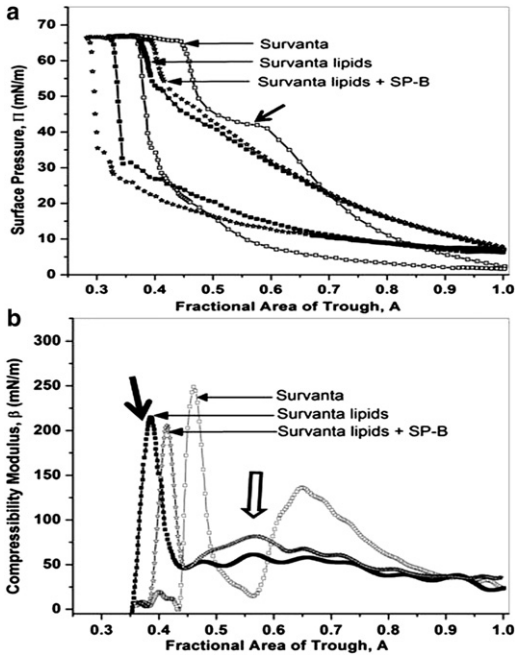

FIGURE 2 (*a*) Surface pressure versus trough area isotherms adsorbed from 800 μg of surfactant in an aqueous dispersion deposited onto a saline buffer subphase. The fourth compression-expansion cycle is shown. (*Open squares*) Survanta shows a characteristic shoulder (*solid arrow*) at 40–45 mN/m where the selective squeeze-out of unsaturated lipids and proteins occurs. The film shows a collapse plateau at Π_{max}~67 mN/m. (*Solid squares*) Lipids extracted from Survanta showing that the characteristic shoulder at ~45 mN/m disappears. Π_{max} remains at 67 mN/m but requires more compression (smaller trough area) to reach the collapse pressure. (*Stars*) Adding 5 wt % SP-B causes the isotherm to shift to larger areas, indicating an increase in adsorption from the subphase. The maximum surface pressure is Π_{max} ~67 mN/m, but at an area in between Survanta and the lipids-only isotherms. (*b*) Compressibility modulus, $\beta = -A(\partial\Pi/\partial A)_T$, evaluated from the isotherms in panel *a*. (*Open squares*) Survanta shows two characteristic peaks followed by sharp dips. The smaller peak at $A = 0.7$ is the squeeze-out plateau. The higher peak at $A = 0.45$ corresponds to monolayer collapse. Moduli > 200 mN/m are associated with L_C or solid condensed films at high surface pressure, due to their semicrystalline order. (*Solid squares*) Removing the proteins decreases the collapse compressibility peak from β ~ 250 to ~215 mN/m (*solid arrow*), although the collapse pressure is unchanged. This may be due to incomplete removal of the more easily compressed L_E phase. At higher trough areas, the compressibility is roughly constant at 50 mN/m and there is no evidence of a squeeze-out peak. (*Stars*) Adding 5 wt % SP-B increases the compressibility up to collapse and restores some features of squeeze-out such as the small peak (*open arrow*). The collapse peak occurs at $A = 0.41$ with a magnitude of 205 mN/m, suggesting that SP-B has minimal effects on monolayer collapse.

maximum was at β ~ 250 mN/m. The compressibility modulus for the film containing SP-B was greater than that of the Survanta lipids up to the collapse peak and shows a small peak (*open arrow*) at the same trough area as the squeeze-out peak of Survanta. The collapse peak with SP-B was at β ~ 205 mN/m, which suggests that SP-B is not involved in monolayer collapse. However, SP-B may assist in the squeeze-out of unsaturated lipids, even though the squeeze-out plateau is not as apparent in the isotherm.

Domain size distribution—effects of SP-B

Fig. 3 shows typical fluorescence images of Survanta lipids without (Fig. 3 *a*) and with (Fig. 3 *b*) SP-B at $\Pi = 24$ (*top*) and 34 mN/m (*bottom*). Discrete dark circular domains are distributed uniformly throughout a continuous bright background, similar to previous observations of model lipid and lipid protein mixtures (16,17,54) and Survanta (21,22). These dark domains are semicrystalline liquid-condensed (L_c) phase (18,21,46,47) made up of closely packed DPPC and palmitic acid that exclude the dye and hence appear dark (18,21,28,46,47). The brighter, liquid-expanded (L_E) phase contains the unsaturated and charged lipids, along with the SP-B (17,27). SP-B led to an increase in the association of surfactant aggregates from the subphase to the monolayer as evidenced by many more bright surfactant aggregates in Fig. 2 *b* compared to Fig. 2 *a*. These aggregates appear to be loosely associated with the LE phase monolayer.

At all surface pressures, SP-B decreased the domain size and increased the number density of domains (Fig. 3). SP-B also decreased the polydispersity (Fig. 4), similar to what was observed when SP-B peptides were added to monolayers made from single lipids and simple lipid mixtures (16,44). The histograms in Fig. 4 quantify the changes in the domain size distributions. Fig. 4, *a–d*, shows that all fits to Eq. 8 had an average R-squared of >0.95. R_o, the minimum energy radius, increases with surface pressure with and without added SP-B much more than the most

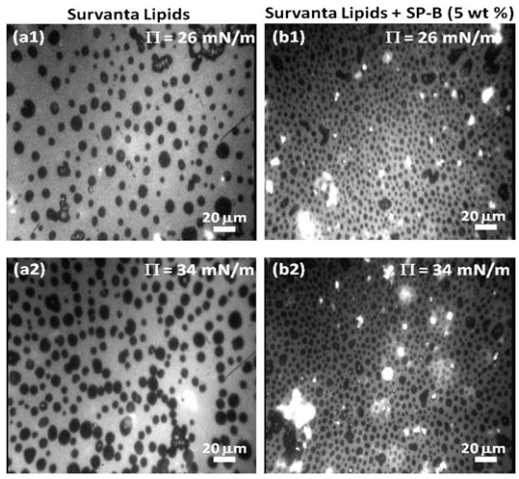

FIGURE 3 Fluorescence microscopy images of (*a*) the lipids extracted from Survanta, and (*b*) the extracted Survanta lipids plus 5 wt % SP-B. (*Top row*) $\Pi = 26$ mN/m; (*bottom row*) Π 34 mN/m. The images show discrete dark L_C phase domains in a continuous bright L_E phase. The domain size decreases and becomes less polydisperse with SP-B (compare *a*1 and *b*1 or *a*2 and *b*2). The domain size and number density also increase with surface pressure (compare *a*1 and *a*2 or *b*1 and *b*2). The bright spots in the images are surfactant bilayer aggregates in the subphase that are attached or associated with the L_E phase of the monolayer. SP-B increases the number of such domains, indicating its role in surfactant transport from the subphase to the interface.

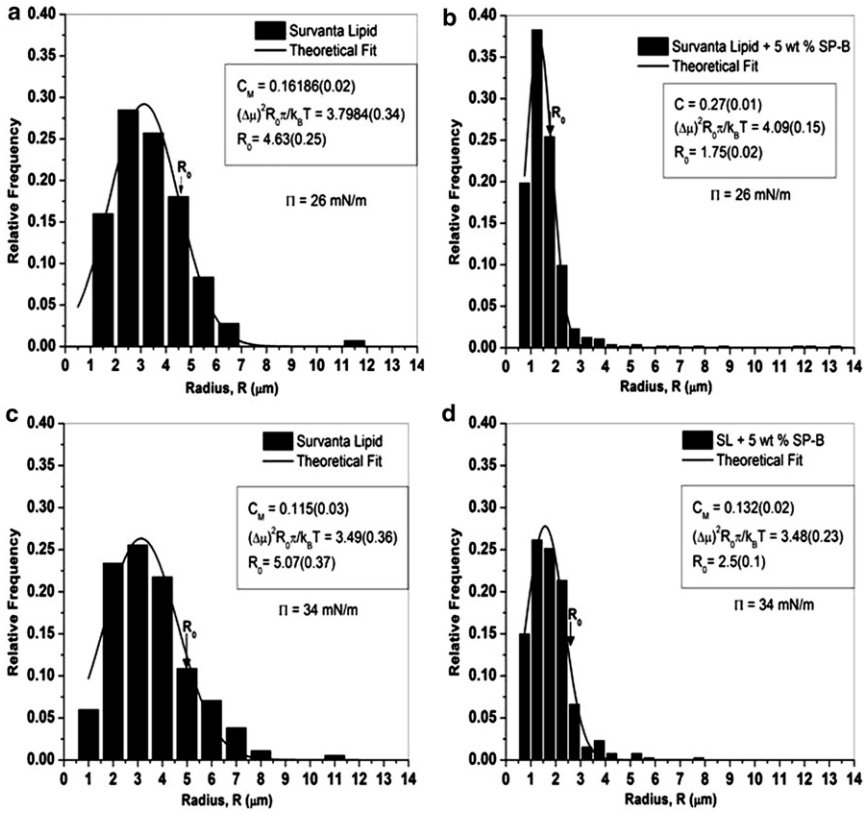

FIGURE 4 Histograms of domain sizes for the images shown in Fig. 3. (*Solid curves*) Theoretical fits using Eq. 8. The three parameters used in the fitting routine were C_M (the fraction of domains of radius R_o), $(\Delta m)^2 R_o/4\varepsilon\varepsilon_0 k_B T = \pi(\Delta\mu)^2 R_o/k_B T$, and R_o (the minimum energy radius from Eq. 2), respectively. Our results show that R_o increases with the surface pressure but decreases with the addition of 5 wt % protein SP-B. Additionally, the polydispersity of the domains (width of the distribution) decreases in the presence of proteins.

probable size, which was roughly constant. The entropy decreases the preferred size of the domain; most domains are smaller than R_o.

Fig. 5 shows the line tension, λ, and the square of the dipole density difference, $(\Delta\mu)^2 = (\Delta m)^2/4\pi\varepsilon\varepsilon_o$ ($(\Delta\mu)^2$ has the same units as λ), determined from the fitting parameters and Eq. 2. For the SP-B containing films, λ and $(\Delta\mu)^2$ are more than a factor-of-two greater than that of the lipids alone at 24 mN/m; however, this difference decreases with increasing surface pressure. For the lipids alone, both λ and $(\Delta\mu)^2$ change little with surface pressure. Fig. 6 shows the increase in λ with SP-B concentration at 26 and 34 mN/m. At the lower surface pressure, the line tension increases linearly with SP-B concentration; however, at 34 mN/m, the line tension reaches saturation at a protein concentration of 1 wt % SP-B, the physiological protein content in native lung surfactants (7).

DISCUSSION

Survanta has a characteristic squeeze-out plateau from $\Pi \sim$ 40 to 45 mN/m (21) in the isotherm in Fig. 2 *a*. This plateau is associated with the reversible removal of unsaturated lipids from the monolayer that are unable to sustain high surface pressures. The squeeze-out effect is also visible in the compressibility modulus (Fig. 2 *b*) as a broad peak of magnitude 140 mN/m, followed by a dip to $\Pi \sim$ 30 mN/m. This squeeze-out allows the surfactant film to go through a refinement process, making it richer in the more-saturated, LC phase components, which in turn leads to a film more resistant to collapse (37). With all proteins present, the unsaturated lipids and proteins squeezed out of the monolayer are held in the vicinity of the interface by the formation of bilayer vesicles and/or multilayer patches (21,22,26,46,55) that act as surfactant reservoirs to ensure the facile reabsorption during inspiration.

Removing the proteins eliminates both the plateau in the isotherm and the peak in the compressibility. It is likely that the unsaturated lipids are removed from the film during the compression, although not in the same way as with the proteins present. The β versus area-curve for the Survanta lipids is roughly constant at $\Pi \sim$ 50 mN/m. This decreased compressibility is likely responsible for the decrease in the trough area at collapse; the area at collapse decreases from 0.45 for Survanta to 0.38 for the Survanta lipids. Adding SP-B causes the reappearance of a slight plateau at $\Pi \sim$ 45 mN/m, which is more visible as a small peak in the compressibility modulus (Fig. 2 *b*), indicating that SP-B may be involved in the reversible refining of the surfactant film. It appears that SP-B is more important to ensuring that the collapse pressure is reached at a smaller compression ratio, than in the absolute value of the collapse pressure, which is constant at $\Pi \sim$ 67 mN/m for all three mixtures.

All three mixtures showed an increase in the two-dimensional isothermal bulk modulus before collapse. Films with a high compressibility modulus have an increased ability to

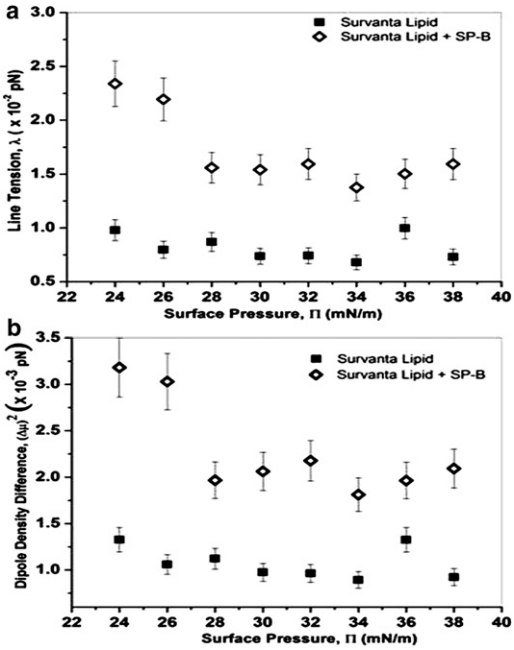

FIGURE 5 (*a*) Line tension, λ, and (*b*) the square of the dipole density difference, $(\Delta\mu)^2 = (\Delta m)^2/4\pi\varepsilon\varepsilon_0$ plotted as a function of surface pressure for Survanta lipids (*solid squares*) and Survanta lipids with 5 wt % SP-B protein (*open diamonds*). Both λ and $(\Delta\mu)^2$ are roughly independent of surface pressure for the Survanta lipids alone. SP-B increases both λ and $(\Delta\mu)^2$ compared to the lipids alone, but the difference decreases with surface pressure, consistent with SP-B being gradually removed with increasing surface pressure.

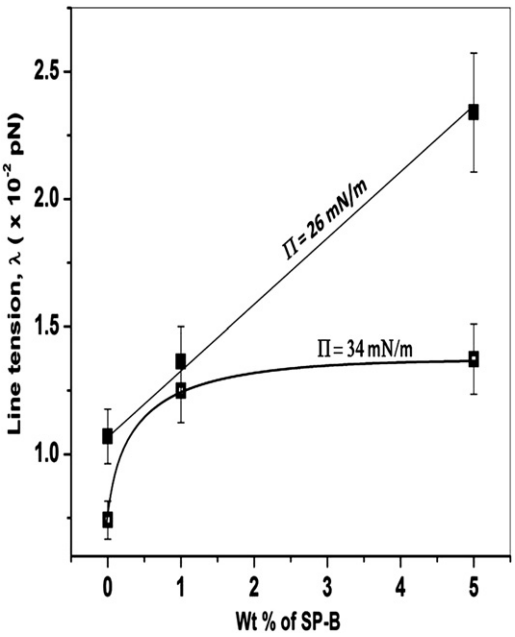

FIGURE 6 Line tension versus protein concentration for $\Pi = 26$ mN/m (*solid squares*) and 34 mN/m (*open squares*). The line tension increases with increasing SP-B concentration at 26 mN/m, but saturates by 34 mN/m. The increase in line tension with SP-B concentration suggests that the SP-B is repelled from the domain boundaries and is soluble in the continuous, fluid L_E phase.

attain significant reductions in the surface tension on compression (14,33–35). The highest moduli are attained in L_C or solid condensed films, at high surface pressure, due to their semicrystalline order (18,21,46,47). Removing the proteins decreases the collapse compressibility peak from ~250 mN/m to ~210 mN/m; restoring SP-B does not increase the peak. This may be due to the changes in the domain size distribution that we see in Figs. 3–6, or due to incomplete removal of the more easily compressed L_E phase. The collapse pressure is unchanged at 67 mN/m.

Figs. 3 and 4 show that SP-B makes a significant difference in the size and polydispersity of the L_C domains. Theoretical analysis of fluorescence images showed that SP-B increased both the line tension, λ, and the dipole density difference, Δm, compared to the values found for the lipids alone. Our Δm ranges from 0.6 to 0.8 Debye/nm, similar to the values obtained by Benvegnu and McConnell (56) by evaluating the Brownian motions of domains trapped within other domains, and by Heinrich et al. (48) determined by evaluating domain boundary fluctuations. The line tension in Survanta lipids found here is an order-of-magnitude lower than those of DMPC-cholesterol monolayers (48,57,58). This is not surprising in that the domain sizes are an order-of-magnitude larger in the DMPC-cholesterol mixtures. However, the values of line tension found here are an order-of-magnitude greater than that between liquid-ordered and liquid-disordered domains in model myelin lipids (30). Complex, multicomponent lipid and protein monolayers are likely to have variations in composition or line active species at the domain boundaries that may smooth the chemical and physical transitions between phases. The line tensions that result may vary by orders of magnitude from femto to tens of picoNewtons, depending on the nature of the transition from one phase to the other (30,59,60).

Both λ and $(\Delta\mu)^2$ are roughly independent of surface pressure for the lipids alone. The DPPC and palmitic acid molecules in the L_C domains undergo a small decrease in tilt on increasing the surface pressure from 20 to 35 mN/m, but the basic lattice is unchanged (18,21,46,47); the lack of change in the lattice of the L_C phase suggests that there is little change in composition of the phase. The LE phase remains disordered throughout this range and also undergoes minimal changes in composition. Hence, there are only small changes in the factors that give rise to λ and $(\Delta\mu)^2$ as the surface pressure increases from 24 to 38 mN/m (30,59,60). This is in contrast to the larger changes of the line tension and dipole density difference between liquid-ordered (L_o) and liquid-disordered (L_d) phases as a miscibility transition or a critical point is approached (29–31,48), where there are relatively large changes in line tension with surface pressure.

The increase in the line tension at all surface pressures with SP-B present may be attributed to a much greater solubility of the protein in the disordered, L_E phase compared to

the ordered, L_C phase. The complex shape of SP-B is incompatible with the crystalline lattice of the LC phase of Survanta (15,21,46) and the protein is expelled from the LC domains. In addition, SP-B has a net positive charge, and the anionic PG is located in the L_E phase (27). X-ray reflectivity measurements have shown that SP-B resides in the more disordered phase at an angle of 56° to the normal (17). The two-dimensional analog to the Gibbs adsorption isotherm (see the Supporting Material) shows that line tension is proportional to the excess concentration of the protein at the domain boundary. A depletion of protein from the domain boundary (negative excess concentration) results in an increase in the line tension between domains (Fig. 5). This is similar to the increase in the surface tension or interfacial tension on the addition of inorganic salts to water; the charged salts are repelled from the air/water or hydrocarbon-water interface and increase the surface or interfacial tension. SP-B is repelled both sterically and electrostatically from the L_C-L_E domain boundary in favor of the bulk L_E phase, causing the line tension to increase.

Insertion of the polycationic SP-B protein into the anionic lipid-containing L_E phase also leads to an increase in the dipole density difference between the L_E and L_C phases. Because the dipole density of the L_C domains should not be affected by SP-B, it is the lipid-protein interactions in the L_E phase that leads to the increased $(\Delta\mu)^2$ or Δm. Interaction between the positively charged proteins with the negatively charged lipid in the L_E phase possibly reduces the net charge density of the L_E phase. This leads to an increase in the dipole-density contrast between the L_C and L_E domains resulting in an increase in $(\Delta\mu)^2$ or Δm. The effect of SP-B decreases with increasing surface pressure; both λ and $(\Delta\mu)^2$ drop almost to the level of the Survanta lipids alone by 38 mN/m. This suggests that SP-B is gradually being removed from the interface—that is, being squeezed-out of the monolayer (27) (the collapse pressure of pure SP-B is ~40 mN/m). Fig. 5 shows that at 34 mN/m, increasing the SP-B concentration from 1 to 5 wt % causes little change in the line tension, while the same change in concentration at 26 mN/m doubles the line tension. This suggests that ~1 wt %, the physiological level of SP-B, is enough to saturate the line tension at higher surface pressures. The conformation or orientation of the SP-B may also change with surface pressure (55), which can alter the dipole strength and cause the observed changes in $(\Delta\mu)^2$.

CONCLUSIONS

While the physiological importance of lung surfactant-specific protein SP-B is clear, its role in modifying the biophysical properties of lipid monolayers is only slowly being understood. The thermodynamic analysis of the domain size distribution presented here provides, to our knowledge, the first simultaneous measurements of the line tension and the dipole density difference between phases in lung surfactant films. SP-B interacts, likely electrostatically, with the anionic lipids in the continuous, fluid L_E phase of the monolayer where its conformation does not interrupt the semicrystalline lattice of the L_C phase. SP-B also promotes the attachment and fusion of bilayer aggregates of surfactant with the monolayer film; these attachments are located within the L_E phase. SP-B increases the line tension and the dipole density difference between the phases in comparison to the lipids alone, which in turn, decreased the mean size and polydispersity of the L_C domains. This change in domain size and polydispersity correlated with an increase in the monolayer two-dimensional isothermal bulk modulus at the surface pressures associated with squeeze-out. The higher compressibility also allows the monolayer to reach the minimum surface tension with less compression of the film area. The line tension increases with SP-B concentration; the two-dimensional Gibbs adsorption isotherm confirms that SP-B is located primarily in the more fluid regions of the lipid films, and avoids the domain boundaries and the ordered L_C domains.

SUPPORTING MATERIAL

Derivation of Gibbs equation at a line interface is available at http://www.biophysj.org/biophysj/supplemental/S0006-3495(11)05358-6.

We thank Professor H. William Taeusch for valuable ongoing collaborations and discussions on lung surfactant function and helpful discussions on monolayer phase behavior and line tension measurements with Sarah Keller and Ben Stottrup.

Support for this work comes from National Institutes of Health grants No. HL-092158 and No. ES-015330 (to A.J.W.), grant No. HL-51177 (to P.D., E.E., A.J.W., and J.A.Z.), and grant No. GM-076709 (to Y.M., A.R., D.W.L., J.A.Z., and J.N.I.).

REFERENCES

1. Avery, M. E., and J. Mead. 1959. Surface properties in relation to atelectasis and hyaline membrane disease. *AMA J. Dis. Child.* 97:517–523.
2. Clements, J. A. 1962. Surface phenomena in relation to pulmonary function. *Physiologist.* 5:11–28.
3. Clements, J. A., and M. E. Avery. 1998. Lung surfactant and neonatal respiratory distress syndrome. *Am. J. Respir. Crit. Care Med.* 157:S59–S66.
4. Pérez-Gil, J. 2008. Structure of pulmonary surfactant membranes and films: the role of proteins and lipid-protein interactions. *Biochim. Biophys. Acta.* 1778:1676–1695.
5. Zuo, Y. Y., R. A. Veldhuizen, …, F. Possmayer. 2008. Current perspectives in pulmonary surfactant—inhibition, enhancement and evaluation. *Biochim. Biophys. Acta.* 1778:1947–1977.
6. Zasadzinski, J. A., P. C. Stenger, …, P. Dhar. 2010. Overcoming rapid inactivation of lung surfactant: analogies between competitive adsorption and colloid stability. *Biochim. Biophys. Acta.* 1798:801–828.
7. Bernhard, W., J. Mottaghian, …, C. F. Poets. 2000. Commercial versus native surfactants. Surface activity, molecular components, and the effect of calcium. *Am. J. Respir. Crit. Care Med.* 162:1524–1533.
8. Clark, J. C., S. E. Wert, …, J. A. Whitsett. 1995. Targeted disruption of the surfactant protein B gene disrupts surfactant homeostasis, causing respiratory failure in newborn mice. *Proc. Natl. Acad. Sci. USA.* 92:7794–7798.

9. Klein, J. M., M. W. Thompson, …, L. M. Nogee. 1998. Transient surfactant protein B deficiency in a term infant with severe respiratory failure. *J. Pediatr.* 132:244–248.
10. Glasser, S. W., M. S. Burhans, …, J. A. Whitsett. 2001. Altered stability of pulmonary surfactant in SP-C-deficient mice. *Proc. Natl. Acad. Sci. USA.* 98:6366–6371.
11. Glasser, S. W., E. A. Detmer, …, J. A. Whitsett. 2003. Pneumonitis and emphysema in sp-C gene targeted mice. *J. Biol. Chem.* 278:14291–14298.
12. Crouch, E., and J. R. Wright. 2001. Surfactant proteins a and d and pulmonary host defense. *Annu. Rev. Physiol.* 63:521–554.
13. Korfhagen, T. R., M. D. Bruno, …, J. A. Whitsett. 1996. Altered surfactant function and structure in SP-A gene targeted mice. *Proc. Natl. Acad. Sci. USA.* 93:9594–9599.
14. Lee, K. Y. C. 2008. Collapse mechanisms of Langmuir monolayers. *Annu. Rev. Phys. Chem.* 59:771–791.
15. Longo, M. L., A. M. Bisagno, …, A. J. Waring. 1993. A function of lung surfactant protein SP-B. *Science.* 261:453–456.
16. Lee, K. Y. C., M. M. Lipp, …, A. J. Waring. 1997. Effects of lung surfactant specific protein SP-B and model SP-B peptide on lipid monolayers at the air-water interface. *Coll. Surf. A.* 128:225–242.
17. Takamoto, D. Y., M. M. Lipp, …, J. A. Zasadzinski. 2001. Interaction of lung surfactant proteins with anionic phospholipids. *Biophys. J.* 81: 153–169.
18. Bringezu, F., J. Q. Ding, …, J. A. Zasadzinski. 2001. Changes in model lung surfactant monolayers induced by palmitic acid. *Langmuir.* 17: 4641–4648.
19. Bringezu, F., J. Q. Ding, …, J. A. Zasadzinski. 2002. Influence of pulmonary surfactant protein B on model lung surfactant monolayers. *Langmuir.* 18:2319–2325.
20. Ding, J. Q., D. Y. Takamoto, …, J. A. Zasadzinski. 2001. Effects of lung surfactant proteins, SP-B and SP-C, and palmitic acid on monolayer stability. *Biophys. J.* 80:2262–2272.
21. Alonso, C., T. Alig, …, J. A. Zasadzinski. 2004. More than a monolayer: relating lung surfactant structure and mechanics to composition. *Biophys. J.* 87:4188–4202.
22. Stenger, P. C., C. Alonso, …, K. E. Pinkerton. 2009. Environmental tobacco smoke effects on lung surfactant film organization. *Biochim. Biophys. Acta.* 1788:358–370.
23. von Nahmen, A., M. Schenk, …, M. Amrein. 1997. The structure of a model pulmonary surfactant as revealed by scanning force microscopy. *Biophys. J.* 72:463–469.
24. Lipp, M. M., K. Y. C. Lee, …, A. J. Waring. 1998. Coexistence of buckled and flat monolayers. *Phys. Rev. Lett.* 81:1650–1653.
25. Schürch, S., F. H. Y. Green, and H. Bachofen. 1998. Formation and structure of surface films: captive bubble surfactometry. *Biochim. Biophys. Acta.* 1408:180–202.
26. Schürch, S., R. Qanbar, …, F. Possmayer. 1995. The surface-associated surfactant reservoir in the alveolar lining. *Biol. Neonate.* 67 (*Suppl 1*): 61–76.
27. Ding, J. Q., I. Doudevski, …, J. A. Zasadzinski. 2003. Nanostructure changes in lung surfactant monolayers induced by interactions between palmitoyloleoylphosphatidylglycerol and surfactant protein B. *Langmuir.* 19:1539–1550.
28. McConnell, H. M. 1991. Structures and transitions in lipid monolayers at the air-water-interface. *Annu. Rev. Phys. Chem.* 42:171–195.
29. Min, Y., T. F. Alig, …, J. A. Zasadzinski. 2011. Critical and off-critical miscibility transitions in model extracellular and cytoplasmic myelin lipid monolayers. *Biophys. J.* 100:1490–1498.
30. Lee, D. W., Y. Min, …, J. A. Zasadzinski. 2011. Relating domain size distribution to line tension and molecular dipole density in model cytoplasmic myelin lipid monolayers. *Proc. Natl. Acad. Sci. USA.* 108: 9425–9430.
31. Honerkamp-Smith, A. R., S. L. Veatch, and S. L. Keller. 2009. An introduction to critical points for biophysicists; observations of compositional heterogeneity in lipid membranes. *Biochim. Biophys. Acta.* 1788:53–63.
32. Diamant, H., T. A. Witten, …, K. Y. C. Lee. 2000. Unstable topography of biphasic surfactant monolayers. *Europhys. Lett.* 52:171–177.
33. Lu, W., C. M. Knobler, …, M. Dennin. 2002. Folding Langmuir monolayers. *Phys. Rev. Lett.* 89:146107.
34. Pocivavsek, L., R. Dellsy, …, E. Cerda. 2008. Stress and fold localization in thin elastic membranes. *Science.* 320:912–916.
35. Pocivavsek, L., S. L. Frey, …, K. Y. Lee. 2008. Lateral stress relaxation and collapse in lipid monolayers. *Soft Matter.* 4:2019–2029.
36. Gopal, A., V. A. Belyi, …, K. Y. Lee. 2006. Microscopic folds and macroscopic jerks in compressed lipid monolayers. *J. Phys. Chem. B.* 110:10220–10223.
37. Gopal, A., and K. Y. C. Lee. 2006. Headgroup percolation and collapse of condensed Langmuir monolayers. *J. Phys. Chem. B.* 110:22079–22087.
38. Ding, J. Q., H. E. Warriner, and J. A. Zasadzinski. 2002. Viscosity of two-dimensional suspensions. *Phys. Rev. Lett.* 88:168102.
39. Choi, S. Y., S. Steltenkamp, …, T. M. Squires. 2011. Active microrheology of phospholipid monolayers: watching domains stretch, flow, yield and heal. *Nature Comm.* 2:312.
40. Kim, K. Y., S. Y. Choi, …, T. M. Squires. 2011. Interfacial rheology of DPPC monolayers at the air-water interface. *Soft Matter.* 10.1039/C1SM05383C.
41. Alonso, C., A. Waring, and J. A. Zasadzinski. 2005. Keeping lung surfactant where it belongs: protein regulation of two-dimensional viscosity. *Biophys. J.* 89:266–273.
42. Brewster, R., P. A. Pincus, and S. A. Safran. 2009. Hybrid lipids as a biological surface-active component. *Biophys. J.* 97:1087–1094.
43. Reference deleted in proof.
44. Lee, K. Y. C., J. Majewski, …, G. S. Smith. 2001. Synchrotron x-ray study of lung surfactant-specific protein SP-B in lipid monolayers. *Biophys. J.* 81:572–585.
45. Nag, K., S. G. Taneva, …, K. M. Keough. 1997. Combinations of fluorescently labeled pulmonary surfactant proteins SP-B and SP-C in phospholipid films. *Biophys. J.* 72:2638–2650.
46. Stenger, P. C., G. Wu, …, J. A. Zasadzinski. 2009. X-ray diffraction and reflectivity validation of the depletion attraction in the competitive adsorption of lung surfactant and albumin. *Biophys. J.* 97:777–786.
47. Lee, K. Y. C., A. Gopal, …, K. Kjaer. 2002. Influence of palmitic acid and hexadecanol on the phase transition temperature and molecular packing of dipalmitoylphosphatidylcholine monolayers at the air-water interface. *J. Chem. Phys.* 116:774–783.
48. Heinrich, M. C., I. Levental, …, T. Baumgart. 2008. Critical exponents for line tension and dipole density difference from lipid monolayer domain boundary fluctuations. *J. Phys. Chem. B.* 112:8063–8068.
49. Hu, Y., K. Y. C. Lee, and J. Israelachvili. 2003. A sealed mini-trough for microscopy and long-term stability studies of Langmuir monolayers. *Langmuir.* 19:100–104.
50. Jung, H.-T., B. Coldren, …, E. W. Kaler. 2001. The origins of stability of spontaneous vesicles. *Proc. Natl. Acad. Sci. USA.* 98:1353–1357.
51. Coldren, B., H.-T. Jung, …, J. A. Zasadzinski. 2003. From vesicle size distributions to bilayer elasticity via cryo-transmission and freeze-fracture electron microscopy. *Langmuir.* 19:5632–5639.
52. Hall, S. B., Z. Wang, and R. H. Notter. 1994. Separation of subfractions of the hydrophobic components of calf lung surfactant. *J. Lipid Res.* 35:1386–1394.
53. Baatz, J. E., Y. Zou, …, R. H. Notter. 2001. High-yield purification of lung surfactant proteins sp-b and sp-c and the effects on surface activity. *Protein Expr. Purif.* 23:180–190.
54. vonNahmen, A., A. Post, …, M. Sieber. 1997. The phase behavior of lipid monolayers containing pulmonary surfactant protein C studied by fluorescence light microscopy. *Eur. Biophys. J. Biophys. Lett.* 26: 359–369.

55. Baoukina, S., and D. P. Tieleman. 2011. Lung surfactant protein SP-B promotes formation of bilayer reservoirs from monolayer and lipid transfer between the interface and subphase. *Biophys. J.* 100:1678–1687.

56. Benvegnu, D. J., and H. M. McConnell. 1993. Surface dipole densities in Langmuir monolayers. *J. Phys. Chem.* 97:6686–6691.

57. Wurlitzer, S., P. Steffen, and T. M. Fischer. 2000. Line tension of Langmuir monolayer phase boundaries determined with optical tweezers. *J. Chem. Phys.* 112:5915–5918.

58. Benvegnu, D. J., and H. M. McConnell. 1992. Line tension between liquid domains in lipid monolayers. *J. Phys. Chem.* 96: 6820–6824.

59. Kuzmin, P. I., S. A. Akimov, …, F. S. Cohen. 2005. Line tension and interaction energies of membrane rafts calculated from lipid splay and tilt. *Biophys. J.* 88:1120–1133.

60. Brewster, R., and S. A. Safran. 2010. Line active hybrid lipids determine domain size in phase separation of saturated and unsaturated lipids. *Biophys. J.* 98:L21–L23.